ACS APPLIED MATERIALS & INTERFACES

Biological and Medical Applications of Materials and Interfaces

Photo-responsive Nanovehicle for Two Independent Wavelength Light-Triggered Sequential Release of P-gp shRNA and Doxorubicin to Optimize and Enhance Synergistic Therapy of Multidrug-resistant Cancer

Ming Wu, Xinyi Lin, Xionghong Tan, Jiong Li, Zuwu Wei, Da Zhang, Youshi Zheng, Ai-Xian Zheng, Bixing Zhao, Yongyi Zeng, Xiaolong Liu, and Jingfeng Liu

ACS Appl. Mater. Interfaces, **Just Accepted Manuscript** • DOI: 10.1021/acsami.8b03823 • Publication Date (Web): 17 May 2018

ACS Publications

is published by the American Chemical Society. 1155 Sixteenth Street N.W., Washington, DC 20036

Photo-responsive Nanovehicle for Two Independent Wavelength Light-Triggered Sequential Release of P-gp shRNA and Doxorubicin to Optimize and Enhance Synergistic Therapy of Multidrug-resistant Cancer

Ming Wu,[†,‡,#] Xinyi Lin,[†,‡,#] Xionghong Tan,[†,‡,§] Jiong Li,[†,‡,§] Zuwu Wei,[†,‡] Da Zhang,[†,‡] Youshi Zheng,[†,‡] Ai-xian Zheng,[†,‡] Bixing Zhao,[†,‡] Yongyi Zeng,[†,‡,⊥] Xiaolong Liu,*[,†,‡] and Jingfeng Liu*[,†,‡,⊥]

[†]The United Innovation of Mengchao Hepatobiliary Technology Key Laboratory of Fujian Province, Mengchao Hepatobiliary Hospital of Fujian Medical University, Fuzhou 350025, P.R. China

[‡]The Liver Center of Fujian Province, Fujian Medical University, Fuzhou 350025, P.R. China

[§] School of Life Sciences, Fujian Agriculture and Forestry University, Fuzhou 350002, P.R. China

[⊥] Liver Disease Center, The First Affiliated Hospital of Fujian Medical University, Fuzhou 350005, P. R. China.

ABSTRACT

Pre-release of RNA molecules than chemotherapeutic drugs with a sufficient interval is a vital prerequisite for RNA/drug co-delivery strategy to overcome multidrug resistance (MDR) of cancer cells, but how to precisely control their release at different time points is still a grand challenge up to now. This study aims to on-demand remotely manipulate RNA and drug release in real time through single delivery system to sequentially play their respective roles for optimizing and enhancing their synergistic antitumor effects. To this end, a photo-responsive mesoporous silica nanoparticle (PMSN) is fabricated as a co-delivery vehicle of P-gp shRNA and photocaged prodrug of doxorubicin, by which the orthogonal and sequential release of shRNA and DOX can be achieved using an external light. In our design, the cationic poly[2-(N,N-dimethylaminoethyl) methacrylate](PDMAEMA) is introduced onto the PMSN surface though a light-sensitive coumarin ester derivative linker to adsorb P-gp shRNA, while the photo-cleavable o-nitrobenzyl ester derivative caged DOX is loaded into the inner pores of the PMSN. The PMSN is found to be effectively internalized by MDR cancer cells, and the release of the shRNA and DOX is demonstrated to be independently regulated by 405 nm and 365 nm light irradiation due to selectively cleaved coumarin and o-nitrobenzyl ester, resulting in enhanced drug retention, and finally bring out optimized and significantly improved chemotherapeutic effects both *in vitro* and *in vivo* for MDR cancer treatment, which might hold extensive application prospects in MDR cancer treatment in future.

KEYWORDS: photo-responsive nanovehicle, sequential release, P-gp shRNA, doxorubicin, multidrug resistance, chemotherapy

INTRODUCTION

Chemotherapy that utilizes antitumor drugs such as doxorubicin (DOX) to inhibit or kill cancer cells is one of main approaches in clinical cancer treatment, but it's efficacy is severely impacted by adverse side effects and the development of multidrug resistance (MDR).[1-2] MDR is regarded as the resistance of tumor cells to various types of chemotherapy drugs with different structural and molecular target. P-glycoprotein (P-gp) recognized as the multidrug resistance protein 1 (MDR1) or ATP-binding cassette sub-family B member 1 (ABCB1), is a type of transmembrane proteins over-expressed in various human cancers to transport the uptaken chemotherapy drugs out of cell across cellular membranes. As a result, this protein will cause decreased drug influx and increased drug efflux, and it is considered to be one of the main protein responsible for MDR.[3-4] P-gp expression can be potentially knockdown through RNA interference (RNAi) which is generally mediated by small interfering RNAs (siRNA) or the precursors to siRNA known as short-hairpin RNAs (shRNA).[1, 5] Therefore, the combination of shRNA therapy and chemotherapy holds great potential to overcome MDR, while the key obstacles remain to achieve simultaneous delivery and stepwise release of RNAs and drugs. On one hand, huge differences in physicochemical properties (i.e. water-solubility, molecular weight, charge, etc.) between anticancer drugs and RNA molecules may result in differences of bio-distribution and tumor accumulation of both types of agents.[6] On the other hand, for reversal MDR, the payload shRNA should be released before the release of chemotherapeutic drug to inactive drug efflux pumps of P-gp, and then subsequently to inhibit the pumping out of uptaken drugs from cancer cells.[7] In recent decades, growing interests have been focused on well-tailored nanocarriers for simultaneous delivery of RNA molecules and chemotherapeutic drugs into the targeted tumor cells to solve problems of their different bio-distribution and tumor accumulation.[8-11] Various kinds of nanocarriers such as polymeric micelles,[12] liposomes,[13] mesoporous silica,[14-15] and other organic or inorganic nanoparticles have been exploited for gene/drug co-delivery.[16-17] Unfortunately, to the best of our knowledge, the currently available carriers cannot satisfy the requirements of strictly controlled release of gene and drugs with an sufficient interval to allow the gene to fully carry out its function, unless the carriers sequentially deliver gene and

drugs in batches;[2, 15-16] While, this might bring the problems of asynchronous bio-distribution and tumor accumulation even using the same carrier. Thus, on-demand manipulation of RNA and drug release through single delivery system to sequentially play their respective roles in real time will be more beneficial for exerting their synergistic antitumor function.

Photo-triggered drug release system (PDRS) manipulated by light provides on-demand release abilities through a high spatial and temporal control manner for activating the therapeutic efficacy. Several types of PDRS have been developed so far, including those based on photochromic groups such as o-nitrobenzyl,[18] coumarin,[19] azobenzene,[20] perylen-3-ylmethanol,[21] p-hydroxyphenacyl,[22] and other miscellaneous groups.[23-24] Among these phototriggers, o-nitrobenzyl and coumarin are two typical orthogonally functional units with wavelength-selective molecular activation charateristics which have been widely exploited for sequentially regulation of biological actions.[25-28] For example, the photolabile diethylamino-coumarin-4-yl (DEACM) group can be cleaved off with 412 nm light illumination but without damaging the nitroveratryloxycarbonyl (NVo) group, and the NVo group could then be removed at 365 nm light.[25] Harnessing these wavelength-dependent photodegradable characteristics of o-nitrobenzyl and coumarin, herein we intend to regulate the release of shRNA and Doxorubicin (DOX) in a sequential manner for optimizing their synergistic therapy in multidrug-resistant cancer cells. To this end, we fabricated mesoporous silica nanoparticles (MSNs) with surface modification of poly[2-(N,N-dimethylaminoethyl) methacrylate] through coumarin linker (MCP) for 405 nm light triggered shRNA release ascribing to the photolysis of coumarin linker at this wavelength. The main reason of choosing cationic PDMAEMA is that they can spontaneously condense gene into compact complexes which might easily escape from endosomes by the proton sponge effect.[29] On the other hand, the hydrophobic prodrug (DOC) of hexadecyl- o-nitrobenzyl derivative caged doxorubicin (DOX) which is loaded into the inner pores of MSNs will become uncaged for light trigged DOX release with 365 nm irradiation.

Therefore, we reported an approach allowing for precisely control the release order of RNA and drugs from a single mesoporous silica nanoparticle only using external light to optimize the synergistic therapy in MDR cancer cells. The selectively and sequentially release of shRNA and DOX depending on two different wavelength light, the sequential release pattern

benefiting for their synergistic therapy in MDR cancer and the relevant mechanisms were investigated both *in vitro* and *in vivo*. The chemical structure and the photolysis of MCP and DOC were presented in Figure 1a, and the sequential release of shRNA and DOX from the nanovehicle regulated by two wavelength light was schematically illustrated in Figure 1b.

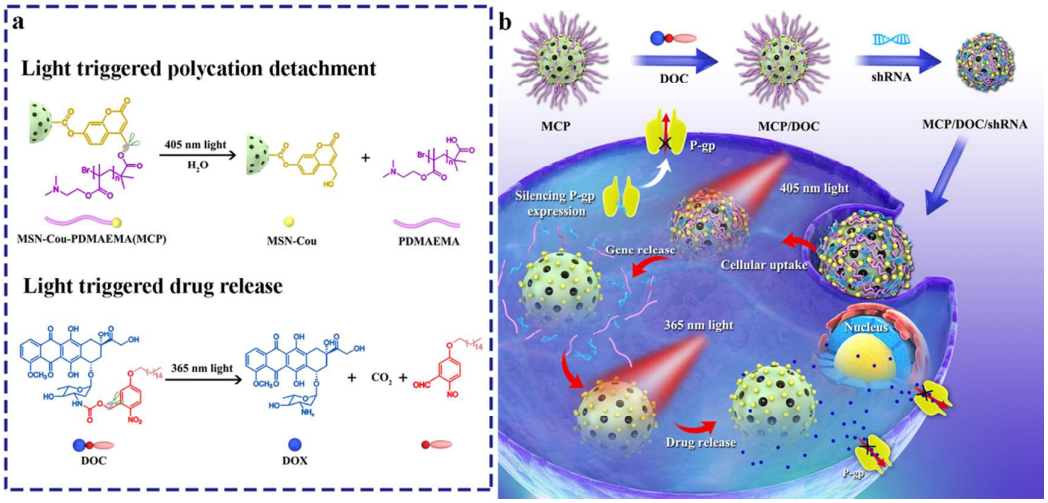

Figure 1. (a) Chemical structure and the photolysis of photoresponsive vehicle (MCP) and DOX prodrug (DOC). (b) Schematic illustration of sequential release of shRNA and DOX regulated by 405 nm and 365 nm light irradiation, using photoresponsive mesoporous silica nanoparticles as co-delivery vehicles for optimizing the synergistic therapy in multidrug-resistant cancer cells.

RESULTS AND DISCUSSION

MSN was synthesized according to the previous method reported by Shi *et al.*[30] As shown in transmission electron microscopy (TEM) image (Figure 2a), the as-prepared MSN exhibited a regular spherical shape, a very uniform particle size distribution around 80-100 nm, a clear mesoporous structure, and very well monodispersity. The surface functionalization of Cou-PDMAEMA on MSN was proceeded through following steps (Figure 2b): (1) the SiO_2 surface was amine-functionalized by APTES (MSN-NH_2),[31] (2) MSN-NH_2 was treated with succinic anhydride to obtain acid-functionalized MSNs (MSN-COOH),[32] (3) MSN-COOH was esterified with 7-hydroxy-4-bromomethyl coumarin (Cou) after activated by $SOCl_2$ (^{1}HNMR and ^{13}CNMR were respectively shown in Supplementary Figure S1 and S2) to obtain coumarin functionalized MSNs (MSN-Cou),[32] (4) MSN-Cou then reacted with 2-bromoisobutyric acid (BIBA), to produce the bromoisobutyryl-terminated MSNs (MSN-Br) as the initiator for subsequent polymerization with DMAEMA though atom transfer radical

polymerization (ATRP) method to obtain the final product of MSN-Cou-PDMAEMA, also named as MCP in this work.[29] The intermediates at each step and the final product of MCP were characterized by fourier transform infrared spectroscopy (FT-IR), UV-Vis absorbance spectra, ^{13}C CP/MAS NMR, thermogravimetric analysis (TGA), dynamic light scattering (DLS), atomic force microscope (AFM) and zeta potential measurement. As an important photolabile intermediate, the FT-IR spectra of MSN-Cou-Br showed two characteristic peaks at 1615 cm^{-1} and 1698 cm^{-1}, ascribing to the C=C bond vibration of benzene and the C=O bond stretching of cyclic ester in the coumarin, respectively, besides the Si-O-Si bond stretching at 1095 cm^{-1} (Figure 2c). Compared with MSN-Cou-Br, a new ester linkage peak around 1731 cm^{-1} was found in the spectra of MCP, which is mainly resulted from the C=O bond stretching of DMAEMA in the PDMAEMA segment (Figure 2c). More intermediates' FT-IR spectra were shown in Figure S3. These results confirmed the successful conjugation of Cou-PDMAEMA on the surface of MSNs. The surface modification with Cou was further confirmed by UV-Vis absorbance spectra. As shown in Figure 2d, the MCP displayed the characteristic absorption band in the region of 240-320 nm. The solid state ^{13}C CP/MAS NMR characterization was also used to determine their chemical compositions. As shown in Figure S4, MSN-Cou-Br showed typical peaks (peak 1, 2, 3) attributed to silane coupling agent[33] and Cou linker (peak 8-16 assigned to benzene carbon atoms).[34] After further conjugation of MSN-Cou-Br with PDMAEMA, the characteristic peaks of PDMAEMA with excessive DMAEMA repeating units were observed from the spectrum of MCP[35] and made the silane and Cou signals negligible in MCP. These results demonstrated the successful conjugation of Cou and PDMAEMA on MCP. The mean hydrodynamic size of bare MSNs measured by DLS was determined to be 115 nm, which was consistent with the result obtained from TEM. The size was further increased to 260 nm after the surface modification of MSNs with Cou-PDMAEMA (Figure 2e), and the zeta potential changed from -18.6 mV (MSN) to 14.9 mV (intermediate MSN-NH_2), -27.3 mV (intermediate MSN-COOH), and 37.4 mV (final product of MCP), respectively (Figure 2f). The size increase of MSN after PDMAEMA conjugation was also verified by atomic force microscope (AFM), as shown in Figure S5. Additionally, TGA was used to determine the content of PDMAEMA in MCP. As shown in Figure 2g, the weight of the intermediates at each step gradually decreased with a

certain amount after successive amine-functionalization, acid-functionalization, acid chloride-functionalization, Cou-esterification, bromoisobutyryl-termination, compared with that of bare MSNs. However, after PDMAEMA conjugation, the MCP exhibited a much higher weight lose of *ca.* 55% wt, which clearly revealed the polymerization of monomer DMAEMA though ATRP method.[29] Before considered as a photoresponsive carrier of shRNA, we selected pDNA as a model gene to evaluate the gene adsorbing ability of cationic MCP *via* electrostatic interaction, and then we employed agarose gel electrophoresis to analyze this process. As shown in Figure 2h, when the N/P ratio, referring to the molar ratio of nitrogen of PDMAEMA on the MSNs to phosphate from pDNA, was above 2.5, the pDNA was completely adsorbed with no electrophoretic shift when comparing with free pDNA. Then, we checked whether shRNA could be condensed into nanometer-sized complex by MCP, which was the main prerequisite for RNA delivery.[15] The MCP/shRNA complex exemplified at N/P ratio of 15 which was also optimal for gene transfection in the later experiments, was selected to analyze its particle size. After condensing of shRNA, the hydrodynamic particle size decreased from 260 to 226 nm (Figure 2e). At this N/P ratio, the nanocomplex showed a positive charge of +29.8 mV. The nanometer size and positively charged surface could facilitate the cellular uptake by endocytosis for subsequent gene transfection.[36]

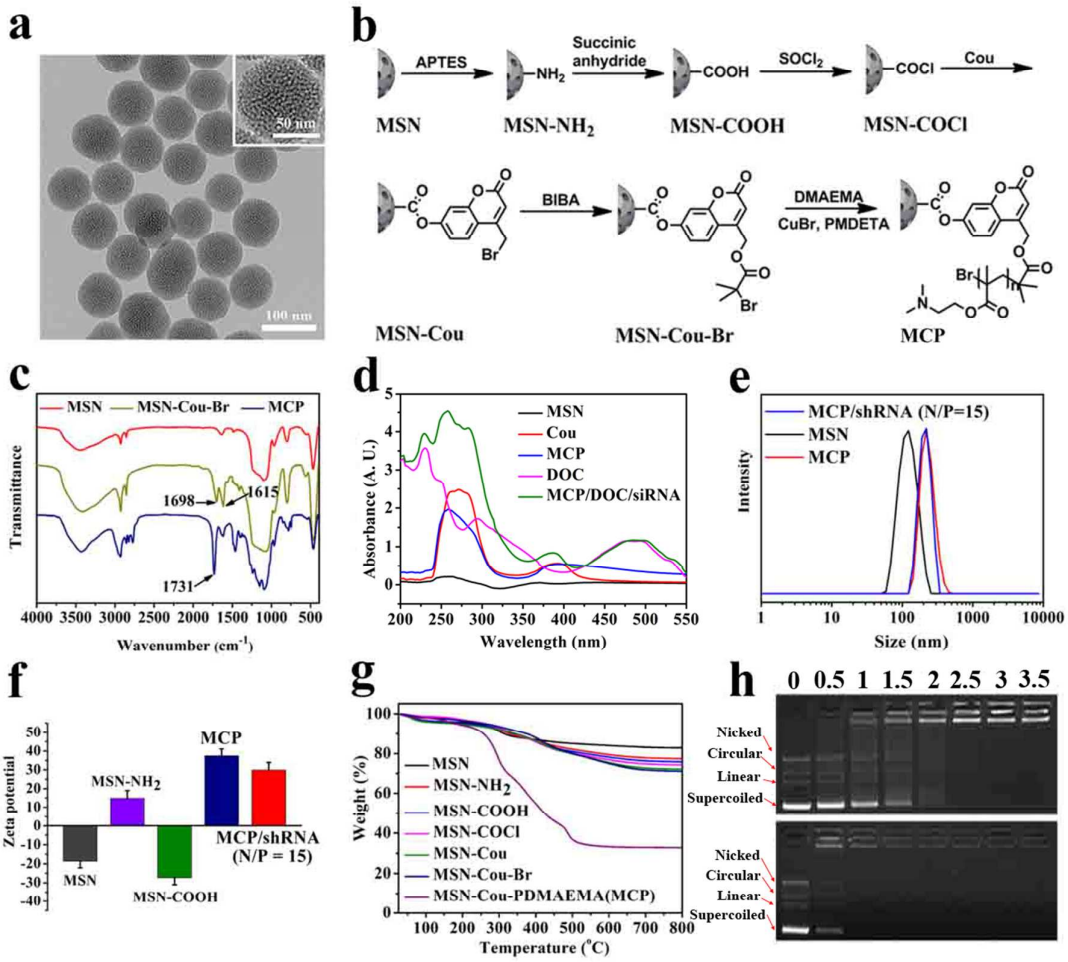

Figure 2. (a) TEM image of MSN. (b) The synthesis procedure of MCP. (c) FT-IR spectra of MSN, MSN-Cou-Br, and MCP. (d) UV-Vis spectra of MSN, Cou, MCP, DOC, and final product of MCP/DOC/siRNA. (e) The size distribution of MSN, MCP, and MCP/shRNA complex at N/P ratio of 15 determined by DLS. (f) The zeta potential of MSN, MSN-NH_2, MSN-COOH, MCP, and MCP/shRNA complex at N/P ratio of 15 determined by DLS. (g) TG curves of MSN, MSN-NH_2, MSN-COOH, MSN-COCl, MSN-Cou, MSN-Cou-Br, and MCP. (h) Electrophoretic mobilities of pDNA complexes with MCP and PEI at different N/P ratios.

To prevent encapsulated DOX from leaking out before triggered by external light of 365 nm wavelength, the photolabile 5-hydroxy-2-nitrobenzyl alcohol was specially conjugated with hexadecyl chain for hydrophobic treatment, and further conjugated with the DOX to form hexadecyl-o-nitrobenzyl derivative caged doxorubicin (DOC, Figure 3a). The structure of DOC and all the intermediates (compound 1 and 2) in the synthetic procedure was characterized by ^{1}HNMR, ^{13}CNMR, verifying the successful preparation of DOC (Figure 3b, c and Figure S6-11). To investigate its photolysis, DOC was dissolved in $CHCl_3$ and undergone 365 nm light irradiation (10 mW/cm^2) for different times, and then was monitored

by thin layer chromatography (TLC). As shown in Figure S12, before exposure to light, DOC showed a single dot at R_f of 0.6, but exposure to 365 nm light irradiation resulted in the formation a distinguishable new dot corresponding to the free DOX at R_f of 0. Almost complete cleavage of DOC prodrug to produce DOX has been clearly proved, even only irradiated for 5 min. Afterwards, DOC was successfully loaded into MCP with a drug loading capacity of 10.2% by physical adsorption through the mesopores,[37] which was determined by fluorescence measurement (Ex= 480 nm, Em= 590 nm) using a calibration curve of DOC fluorescence intensity with various concentrations ranged from 0.0286 μg/mL to 7.34 μg/mL (correlation coefficient of R^2= 0.997), as shown in Figure S13. The final product of MCP/DOC/shRNA was confirmed by UV-Vis absorbance spectra. As shown in Figure 2d, in addition to the characteristic absorption band of coumarin group in the region of 240-320 nm, our MCP/DOC/shRNA also showed a typical absorption band at 400-550 nm, resulting from the absorbance of loaded DOC in MCP.

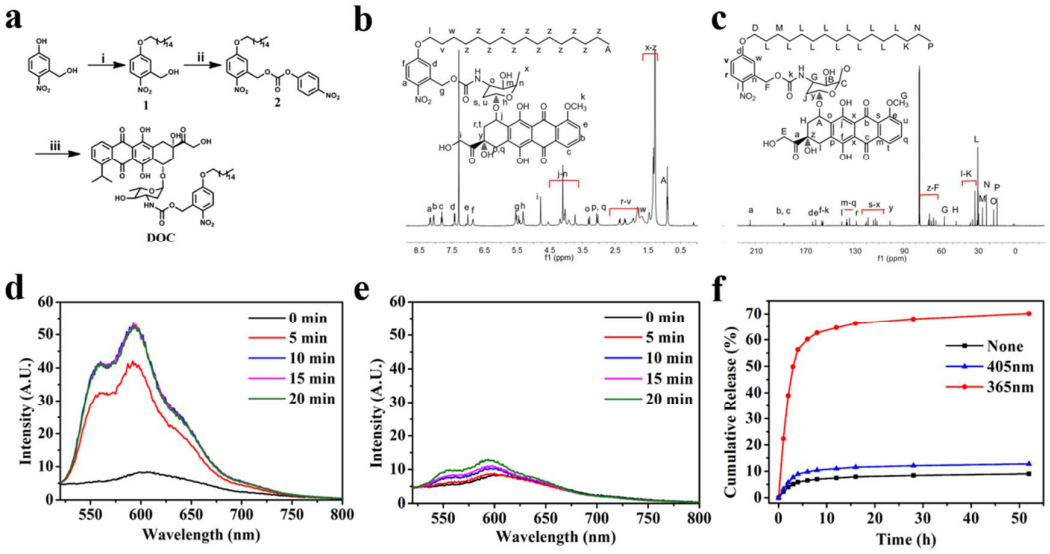

Figure 3. (a) The synthesis procedure of DOC; (i) 1-bromohexadecane, Na_2CO_3; (ii) 4-nitrophenyl chloroformate, DIPEA; (iii) Doxorubicin hydrochloride, Et_3N. ^{1}HNMR (b) and ^{13}CNMR (c) spectra of DOC. Fluorescence spectra of MCP/DOC irradiated with 365 nm light (d) or 405 nm light (e) for various time ranging from 0 to 20 min. (f) *in vitro* release of DOX from MCP/DOC after irradiated with 365 nm light or 405 nm light for 10 min, while none light exposure was used as a control.

Next, we explored the utility of DOC loaded MCP for light-controlled selectively release of free DOX, for which DOC loaded MCP was exposed to 365 and 405 nm light sources separately. As the fluorescence of DOC encapsulated in MCP suffers from significant

quenching due to aggregation-induced fluorescence quenching effect,[38] but after uncaged by light irradiation, the fluorescence of released DOX will recover. Thus, the light-regulated drug release from DOC loaded MCP (MCP/DOC) can be preliminarily analyzed by the fluorescence measurement. As shown in Figure 3d, a sudden increase of fluorescence observed within 5 min irradiation of 365 nm light (10 mW/cm^2) indicated the effective release of DOX into solution. However, under the same conditions, the fluorescence did not obviously increase, even irradiation for 20 min under 405 nm light irradiation (Figure 3e). Then the *in vitro* light triggered drug release profile determined by using a calibration curve of standard DOX fluorescence intensity at various concentrations (Figure S14). As shown in Figure 3f, irradiation of DOC loaded MCP with 365 nm light for 10 min effectively uncaged the DOX from nitrobenzyl derivative, resulting in >60% DOX release within 6 h, and a saturated release percentage around 70% after 16 h. In contrast, only 13% and 9% DOX was released with 405 nm light irradiation or without irradiation even after 48 h, respectively. These results clearly demonstrated the release of DOX in our designed MCP could be selectively regulated by 365 nm light irradiation, while the 405 nm light which used for control gene release has very limited effect on the DOX release. On the other hand, as Cou can be photolysis under 405 nm light which has been preliminarily demonstrated by TLC (Figure S15), we further investigated the photoresponsive gene release resulting from the Cou cleavage under this wavelength. As shown in Figure S16, YOYO-3 labeled pDNA was found to be more easily detached from MCP after light irradiation, as the higher fluorescence intensity of the supernatant of MCP/YOYO-3 labeled pDNA after light irradiation has been observed, comparing with that without light irradiation. Therefore, the sequential release of gene and drug might be feasible when 405 nm light used before 365 nm light with a sufficient interval.

Another vital issue in this work is whether the inhibition of P-gp expression in MDR cancer cells can be manipulated by pre-defined exposure to 405 nm light, which could allow for triggering the release of P-gp shRNA from MCP. For this purpose, HepG2/ADR cells were firstly chosen to assess their utility as a DOX-resistant cancer cell model in our following experiments, through investigating their drug resistance and P-gp expression. As shown in Figure 4a, after incubation with free DOX for 48 h, HepG2/ADR cells exhibited an obvious

drug resistance with the half maximal inhibitory concentration (IC_{50}) of 15.8 μg/mL, which was much higher than that of nonresistant HepG2 cells (IC_{50}=0.9 μg/mL). Meanwhile, the P-gp expression in these two types of cells was also evaluated though western blot analysis. As expect, the expression level of P-gp in HepG2/ADR cells was significantly higher as compared with HepG2 cells (Figure 4b).

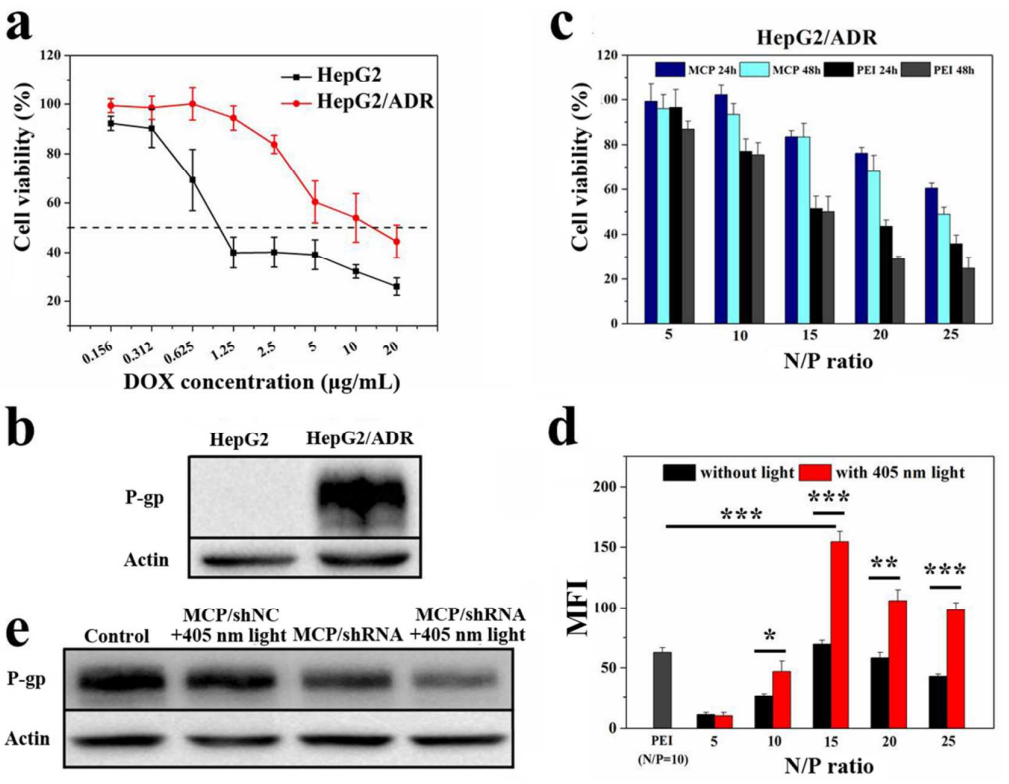

Figure 4. (a) Cell viability of HepG2 and HepG2/ADR cells treated with different concentration of DOX for 48 h. (b) P-gp protein expression determined by Western blot analysis in HepG2 and HepG2/ADR cells, while actin was used an internal reference. (c) *In vitro* cytotoxicity of MCP at different N/P ratios against HepG2/ADR cells after being cultured for 24 or 48 h, while PEI was used as a control. (d) EGFP gene expression mediated by MCP in the presence or absence of 405 nm light, at different N/P ratios in HepG2/ADR cells, as measured through flow cytometry. The MFI value was calculated after the non-treated cells as the benchmark. p values were calculated using ANOVA with post-hoc tests (*$p < 0.05$, **$p < 0.01$, ***$p < 0.001$; $n = 3$ per group). (e) P-gp protein expression determined by Western blot analysis in HepG2/ADR cells incubated with MCP/shNC followed by 405 nm light exposure, MCP/shRNA without light exposure, or MCP/shRNA followed by 405 nm light exposure.

Nanoparticles with positive zeta potential could more easily attach to negatively charged cell membranes, however, like a double-edged sword, this also will bring high cytotoxicity. Therefore, the tolerable cytotoxicity is an important criterion for any polycation gene vector.

In this case, we evaluated the cytotoxicity of MCP on HepG2/ADR cells through CCK8 assay, and compared it with non-viral gold gene carrier standard of PEI (25 kDa). As shown in Figure 4c, MCP showed much lower cytotoxicity than PEI at all the N/P ration, after incubation with the HepG2/ADR cells for 24 or 48 h. Another important index for gene vector is that they should be efficiently uptaken by cells and escape from endosomes/ lysosomes before release of payloads for displaying therapeutic effect.[39] Thus, the intracellular localization of MCP/pDNA complex was observed by confocal laser scanning microscopy (CLSM) while the pDNA and lysosomes were labeled by YOYO-3 and Lysotracker DND-26, respectively. As shown in Figure S17, large amount of red fluorescence of gene were observed inside the cell and mostly co-localized with lysosomes, after 2 h incubation. However, the green fluorescence of lysosomes disappeared after 4 h incubation, implying their destruction caused by the proton sponge effect of PDMAEMA in MCP.[36] These results demonstrated that our nanovehicles could effectively deliver gene into cells and escape from lysosomes.

Before investigation of the knockdown efficiency of P-gp expression by MCP/shRNA under 405 nm light exposure, we analyzed the gene transfection efficiency mediated by our nanoparticle using plasmid pCDH-CMV-EF1α-EGFP (pEGFP) as reporter gene in HepG2/ADR cells. the gene transfection efficiency of MCP/pEGFP was first quantitatively studied by flow cytometry experiments, and the gene expression levels were reflected by the mean fluorescence intensity (MFI) of the treated cells, after subtracted the value of the non-treated cells. Meanwhile, as a standard polymeric gene delivery system, PEI/pEGFP complex at its optimal N/P ratio of 10 was used as a control.[29, 36] As shown in Figure 4d, the MCP/pEGFP complex exhibited a maximum transfection efficiency at N/P ration of 15. When the N/P ratio was above 15, the transfection efficiency decreased which might be ascribed to the significant cytotoxicity at higher N/P ration. However, under the same conditions, when the MCP/pEGFP complex treated cells were exposed to 405 nm laser (10 mW/cm^2) of 10 min, the transfection efficiency was much higher than that without light irradiation, at the N/P ratios ranging from 10 to 25. It was encouraging that the transfection efficiency of MCP/pEGFP at N/P ratio of 15 was even higher than that of PEI/pEGFP at its optimal N/P ratio of 10. These results indicated that our MCP as a photoresponsive vector for

405 nm light triggered gene release was even superior than PEI (25 kDa) with respect to the transfection efficiency and biocompatiblity. The gene transfection efficiency of MCP manipulated by 405 nm light was further confirmed through direct visualizing green fluorescence of EGFP in the transfected cells by a fluorescence microscope. As shown in Figure S18, more EGFP (higher green fluorescence) was expressed with 405 nm light irradiation (10 mW/cm^2) for 10 min, compared with the group without light irradiation. Light irradiated cells at N/P ratio of 15 exhibited the highest fluorescence signals, which was consistent with the results of flow cytometric analysis. Although the gene expression level without photoirradiation at N/P ratio of 15 seems comparable with that of the standard PEI (N/P ratio of 10), the gene expression level of this non-viral carrier is still not high, especially compared with the viral vector often used in gene transfection. Therefore, photocontrol gene release for enhanced intracellular transfection which will ultimately promote the P-gp silencing efficiency, as demonstrated in our work, is still worthy to develop. Therefore, MCP/gene at N/P ratio of 15 was used in the following experiments. These results indicated that the gene release could be accelerated for enhancing their biological function by 405 nm light irradiation. Based on this, we next studied the ability of MCP/shRNA complex to silence the P-gp expression, which was manipulated by 405 nm light. The P-gp targeted shRNA (denoted as shRNA) was used for this purpose, while scrambled shRNA was used as an negative control (denoted as shNC). As shown in Figure 4e, HepG2/ADR cells incubated with MCP/shNC and subsequently irradiated with 405 nm light showed similar P-gp level with the control cells without any treatment, which means both of MCP and 405 nm light irradiation alone had no effect on P-gp expression of HepG2/ADR cells. However, when the MCPs were condensed with shRNA, the P-gp level was effectively suppressed, and more evident with 405 nm light irradiation. This data indicate that our MCP not only can efficiently deliver the shRNA, while the delivered shRNA also can be rapidly released for inhibiting the P-gp expression triggering by external 405 nm light irradiation. Although phenol (especially phenolate) moiety is considered to be important for the efficient photochemical cleavage reaction of coumarin derivatives as a caged group, while the coumarin moiety of the nanoparticle in the ester form is still feasible as a photo-trigger, because esterified coumarin moiety or other chemical groups like tertiary amine has also been demonstrated to be

effectively photo-cleaved.[32, 40-41] As mentioned before, the co-delivery and sequential release of shRNA and drug will benefit the retention of drug in MDR cancer cells through inhibiting P-gp activity by shRNA. Therefore, we evaluated the influence of release order of shRNA and DOX on the DOX retention in HepG2/ADR cells through adjusting the light irradiation order, for which the cells incubated with MCP/DOC/shRNA was treated by different light exposure and then visualized by confocal laser scanning microscopy (CLSM). As shown in Figure 5a, without light irradiation, the MCP/DOC/shRNA treated cells did not show any released DOX fluorescence (red, group iii), compared with the non-treated cells (group i), demonstrating the very slight drug release without light exposure. With the usage of a single 405 nm light, the MCP/DOC/shRNA treated cells still showed a very weak red fluorescence, suggesting that 405 nm light irradiation had limited effect on DOX release (group iv). However, when a single 365 nm light was used, the treated cells exhibited a much higher red fluorescence signal than that under 405 nm light irradiation (group v), indicating the 365 nm light could effectively trigger DOX release. These results were consistent with the *in vitro* drug release results, and further demonstrated that the DOX release could be selectively triggered by 365 nm light irradiation, while 405 nm light used for gene release has very limited effect in this case. To further illustrate the importance of the sequential release of shRNA and DOX, MCP/DOC/shRNA treated cells underwent 365 and 405 nm simultaneous light irradiation (group vi) or pre 405 nm and post 365 nm irradiation with an interval of 24 h to guarantee the pre-released shRNA taking its role in reversal of drug resistance (group vii). Before comparing these two groups, it should be noteworthy that the results in group v and vi are very similar with a comparable red florescence mainly located in the cytoplasm even though 365 and 405 nm light simultaneously usage in group vi, which might be ascribed that the Cou group for regulating shRNA release could be cleaved at both 365 and 405 nm light irradiation.[21] But this prosperity has no impact on successive shRNA and DOX release regulated by pre 405 nm and post 365 nm light in our case, as the DOX can not release under pre 405 nm irradiation. As expected, the fluorescence of DOX in group vii was much stronger compared with any other groups, and a strong red signal was clearly observed in the nuclei (white arrows) for raising the anticancer effects *via* its intercalation with DNA backbone,[42-44] because the pre-released shRNA had been endowed a relatively sufficient time to complete

suppressing the P-gp expression for facilitating the accumulation of post-released DOX at this condition, while dual-light simultaneous irradiation (group vi) could not exert this synergistic effect completely. Furthermore, the cells treated with the nanocomplex carried with scrambled shRNA (MCP/DOC/shNC) was also used as a control to demonstrated the released shRNA could silence the P-gp for enhancing the DOX retention, as still a very weak fluorescence in control cells (group viii), although both 365 nm light and 405nm light were also sequentially used to trigger the shNC and drug release. Taken together, these CLSM results clearly demonstrate that the sequential release of shRNA and DOX regulated by an ordered exposure to lights of 405 nm and 365 nm can optimize the drug accumulation in MDR cells.

To further investigate the influence of time intervals between two light irradiation on the efficiency of P-gp expression silencing, the HepG2/ADR cells were incubated with MCP/DOC/shRNA complexes for 5 hours to allow the sufficient cellular uptake, then were irradiated by 405 nm light for 10 min, subsequently followed by the 365 nm light irradiation at different intervals including 0 hours, 2 hours, 6 hours, and 19 hours. Afterwards, the P-gp protein expression as well as the cell viability were analyzed. As shown in Figure S20a, the P-gp protein expression can not be silenced without any time interval (interval of 0 hours), since the shRNA need time to exert its functions; while as increase the time intervals, the P-gp protein expression has been gradually silenced, and almost achieved a complete inhibition of P-gp expression after 19 hours, due to the sufficient working time of released shRNA. Consequently, effective drug resistant cancer cell killing has also been achieved after 19 hours of time interval (Figure S20b). Therefore, the time interval of 19 hours has been applied for following *in vitro and in vivo* studies.

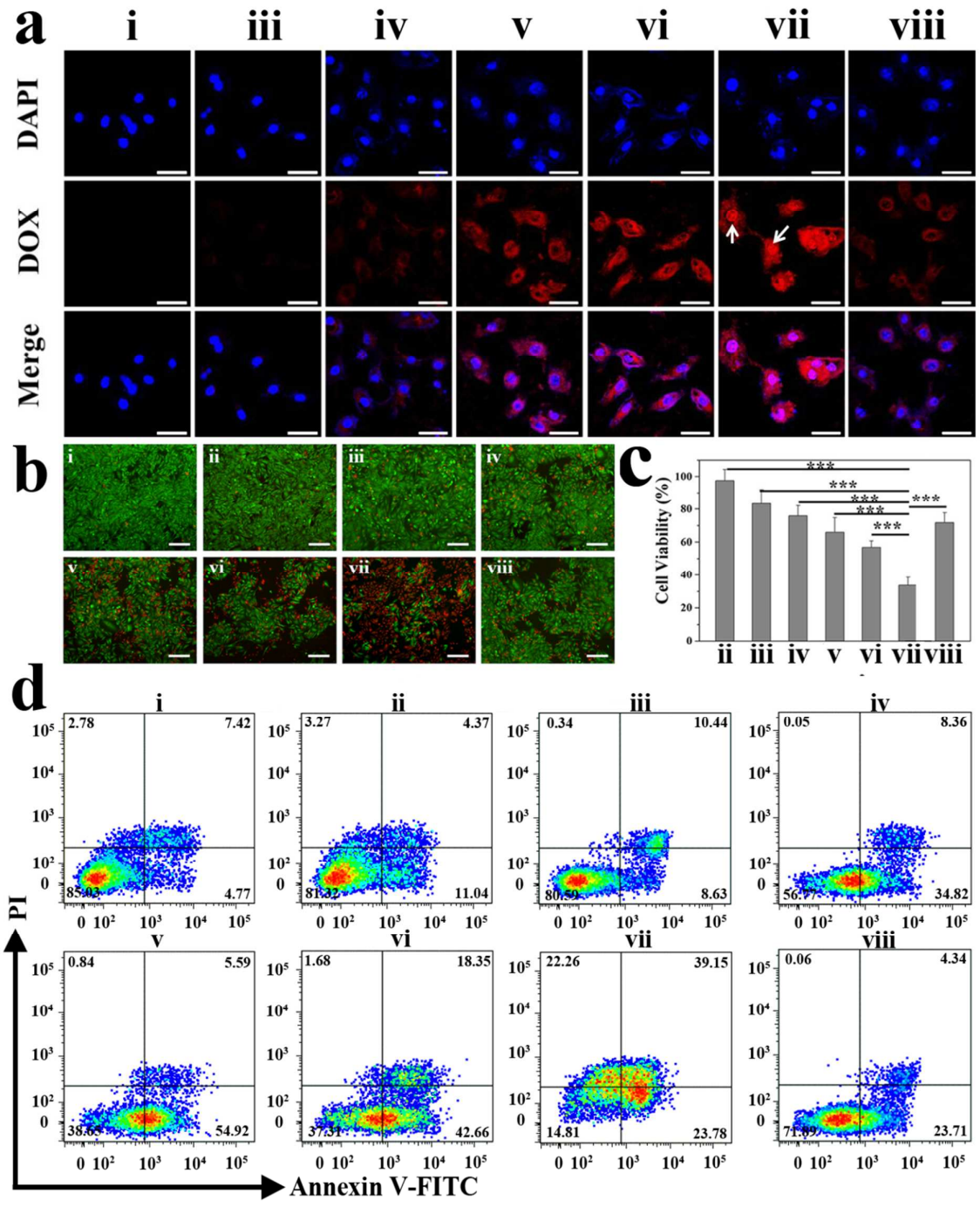

Figure 5. (a) CLSM images of HepG2/ADR cells with different treatments. Scale bar is 20 μm. (b) Fuorescence microscopic images of HepG2/ADR cells stained by the live/dead cell staining kit with different treatments. Scale bar is 50 μm. (c) Cell viability of HepG2/ADR cells with different treatments, measured through CCK8 assay. p values were calculated using ANOVA with post-hoc tests (* $p < 0.05$, ** $p < 0.01$, *** $p < 0.001$; $n = 4$ per group). (d) Flow cytometry analysis of HepG2/ADR cell apoptosis induced by different treatments as indicated using Annexin V-FITC/PI apoptosis detection assay. (i) blank control; (ii) with 365

and 405 simultaneous light irradiation; (iii) MCP/DOC/shRNA without light irradiation; (iv) MCP/DOC/shRNA with 405 nm light irradiation; (v) MCP/DOC/shRNA with 365 light irradiation; (vi) MCP/DOC/shRNA with 365 and 405 nm simultaneous light irradiation; (vii) MCP/DOC/shRNA with pre 405 nm and post 365 nm irradiation; (viii) MCP/DOC/shNC with pre 405 nm and post 365 nm irradiation.

Another major goal of our investigation is to examine whether the co-delivery and sequential release of shRNA and DOX can exert their optimized synergistic antitumor efficacy on MDR cells. For this purpose, HepG2/ADR cells with different treatments was stained with LIVE/DEAD Cell Vitality Assay Kit, in which the live cells and dead cells could be discriminated though observation of green and red fluorescent cells, respectively. As shown in Figure 5b, dual 405 and 365 nm light irradiation (group ii) showed negligible phototoxicity against HepG2/ADR cells, as an entire green fluorescence in the cells. Meanwhile, in the absence of light irradiation, the cells treated with MCP/DOC/shRNA (group iii) also showed a very little red fluorescence of dead cells, demonstrating the good biocompatibility of our MCP and hardly release of shRNA and DOX without light triggering. In addition, the cell death treated with MCP/DOC/shRNA and 405 nm light irradiation (group iv) was still not obvious, compared with the cells treated with the same nanocomplex but with 365 nm (group v) or simultaneous 405 nm and 365 nm light irradiation (group vi), owing to the accelerating drug release under 365 nm light exposure rather than 405 nm light exposure. However, we found the sequential release of shRNA and DOX from MCP/DOC/shRNA complexes regulated by pre 405 nm and post 365 nm light irradiation (group vii) showed a most significant synergistic effects on killing cancer cells, most likely due to rapid downregulation of P-gp expression by shRNA before triggered DOX release, thereby facilitating the drug retention in the cells. By comparison, MCP/DOC/shNC (group viii) showed much less cytotoxicity than MCP/DOC/shRNA in the presence of pre 405 nm and post 365 nm light irradiation, as evidenced by limited red fluorescence of dead cells in this group. The synergistic antitumor effects of sequential delivery of shRNA and DOX was further quantitatively analyzed using CCK8 assay. As shown in Figure 5c, at the same dose, MCP/DOC/shRNA with pre 405 nm and post 365 nm light (group vii) irradiation showed a significantly enhanced cytotoxicity by decreasing the cell viability to 33%, while the cell viabilities in other group was much higher than this group, which was in accordance with that

obtained from the LIVE/DEAD Cell Vitality Assay in Figure 5b. We further analyzed whether the cell killing of our MCP/DOC/shRNA was through the cell apoptosis pathway, which was determined by flow cytometry using Annexin V-FITC/PI apoptosis detection assay. As shown in Figure 5d, only light irradiation (group ii) or MCP/DOC/shRNA (group iii) incubation has little effect on cell apoptosis. However, once the MCP/DOC/shRNA-incubated cells were irradiated with external light, the percentages of early and late apoptotic cells significantly increased to be 34.82% and 8.36% in group iv, 54.92% and 5.59% in group v, and 42.66% and 18.35% in group vi. Most obviously, the percentages of late apoptotic cells (39.15%) and necrotic cells (22.26%) in group vii, whose cells were incubated with MCP/DOC/shRNA in the presence of pre 405 nm and post 365 nm irradiation, were much higher than the cells in other groups. Overall, these results clearly suggested that co-delivery and sequential release of shRNA and DOX regulated by pre 405 nm and post 365 nm light, can exert enhanced synergistic antitumor efficacy on MDR cells *via* inducing cell apoptosis, which might be resulted from the higher drug retention in this condition.

Based on the aforementioned *in vitro* results, it is anticipated that the enhanced drug retention *via* sequential release of shRNA and DOX triggered by ordered 405 nm and 365 nm light will benefit the *in vivo* treatment of MDR solid tumor. Before the *in vivo* study, we have further investigated the penetration depth and photo-damage effect of both 405 nm and 365 nm light, to ensure the lights could penetrate into the tumor and attenuate the photo-damage of light itself. As shown in Figure S21a, the penetration depth of light was determined by the attenuation of light power density after passing through pork with various thicknesses; although the light power densities attenuate dramatically with the increase of tissue thickness, the power densities of both 365 nm and 405 nm light could still maintain 1.9% (19 mW/cm^2) and 3.4 % (34 mW/cm^2) of original received power even after passing through 5mm thickness pork tissue, respectively. Considering that the diameter of subcutaneous tumor model with a volume of ~50 mm^3 is less than 5 mm and the light power intensity of 10 mW/cm^2 can effectively work as demonstrated *in vitro*, then 1 W/cm^2 power intensity was chosen for our following *in vivo* studies. Afterwards, the photo-damage effect of such relatively strong light exposure was also further investigated by exposing the Balb/c-nude mice to 405 nm and 365 nm light irradiation with the power intensity of 1 W/cm^2 for various

times ranged from 2.5 min to 10 min; then, the skin tissues under light exposure were checked by H&E staining. As shown in Figure S21b, there were no significant pathological changes of the exposed skin tissues as compared with the control group without light irradiation, implying that 10 minutes irradiation under 1 W/cm^2 is relatively safe and has no obvious photo-damage.

To further investigate the *in vivo* therapeutic efficacy, the mice bearing a subcutaneous HepG2/ADR xenograft were randomly divided into 8 groups with different treatments as detailed in "MATERIALS AND METHODS" section, and the typical therapeutic procedures were schematically illustrated in Figure 6a. According to the digital photos and the tumor volume variation profiles (Figure 6b), a significant inhibition of tumor growth at day 24 could be observed in groups of v, vi and vii that received MCP/DOC/shRNA treatment incorporating 365 nm light irradiation, compared with the control group (i), light irradiation only group (ii), MCP/DOC/shRNA only group (iii) and MCP/DOC/shRNA with 405 nm light irradiation group (iv), because of the selectively photoregulated drug release upon 365 nm light irradiation. Among these three groups (v, vi and vii) with apparent therapeutic effects, the mice treated with MCP/DOC/shRNA plus pre 405 and post 365 nm irradiation (group vii) showed most significant therapeutic outcome, suggesting the importance of release sequence of shRNA and DOX for optimizing the synergistic effect. By comparison, MCP/DOC/shNC group with pre 405 and post 365 nm irradiation (viii) showed much lower tumor growth inhibition ability, due to P-gp which is responsible for drug efflux would not be suppressed by shNC. However, the difference between the treatments with simultaneous (group vi) and sequential irradiation (group vii) looks relatively small, which might be ascribed to co-released shRNA and drug also exert some combination effect, as reported by other literatures.[1-2, 17] With further optimizing light energy or nanoparticles dosage, we believe the their synergistic effect benefited from the sequential release manner will be maximized for the proposal of new therapies. The therapeutic efficiency was also confirmed by the average tumor weight (Figure 6c), which was consistent with the relative tumor volume results. From the pathological images of tumor tissue with hematoxylin and eosin (H&E) staining (Figure 6d), the typical characteristics correlated with necrosis, such as cytoskeleton collapse and nucleus dissociation, were most obvious in group vii comparing with any other groups; and

these results were also well consistent with the tumor growth or tumor weight results.

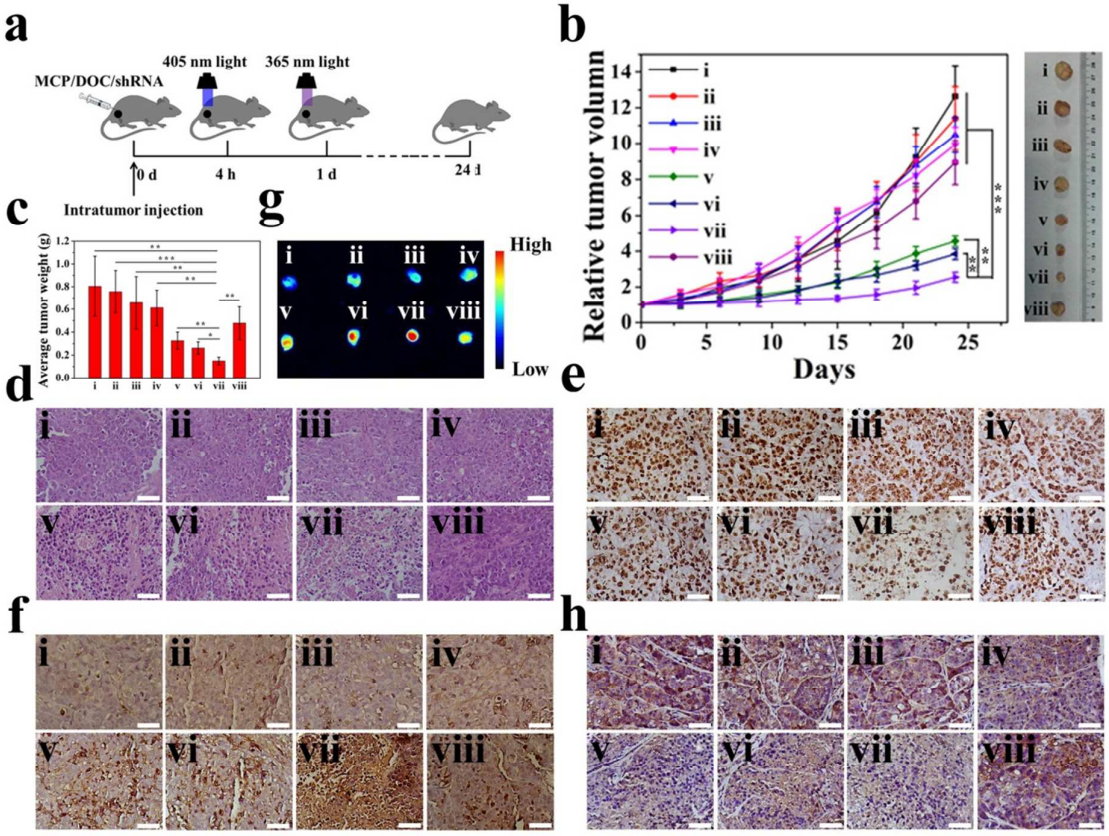

Figure 6. In vivo antitumor effects of MCP/DOC/shRNA in a mouse model. (a) schematic illustration of the typical therapeutic procedures (group vii). Relative tumor volume and representative tumor images (b) and average tumor weight (c) after various treatments as indicated. p values were calculated using ANOVA with post-hoc tests (* $p < 0.05$, ** $p < 0.01$, *** $p < 0.001$; $n = 4$ per group). Optical microscopic images of tumor slices stained by H&E (d), PCNA immunohistochemistry (e), and TUNEL (f) after indicated treatments in different groups. Scale bar is 100 μm. (g) Tumor tissue imaging at 3 days-post injection. The excitation wavelength of DOX was 488 nm. (h) Optical microscopic images of tumor slices stained by P-gp immunohistochemistry at 3 days-post injection (Scale bar: 50 μm). PBS (i), PBS with 365 and 405 simultaneous light irradiation (ii), MCP/DOC/shRNA (iii), MCP/DOC/shRNA with 405 nm light irradiation (iv), MCP/DOC/shRNA with 365 light irradiation (v), MCP/DOC/shRNA with 365 and 405 nm simultaneous light irradiation (vi), MCP/DOC/shRNA with pre 405 nm and post 365 nm irradiation(vii), MCP/DOC/shNC with pre 405 nm and post 365 nm irradiation (viii).

To further identify the molecular mechanisms responsible for the therapeutic efficacy of MCP/DOC/shRNA treatment *in vivo*, proliferating cell nuclear antigen (PCNA) immunohistochemistry and TUNEL staining were systematically analyzed for tumor tissue in different groups. As shown in Figure 6e and Figure 6f, the minimal proliferating cells *via* PCNA assay along with the maximal apoptotic cells *via* TUNEL assay were also observed in

group vii. Compared with other groups, the most excellent therapeutic effect against HepG2/ADR tumor in group vii might be ascribed to the largest retention of drug in tumor *via* controlled drug release after suppression of the P-gp expression evoking by shRNA (Figure 6g).

The P-gp protein being down-regulated by RNA silencing has been well recognized as an effective strategy for MDR reversal by enhancing drug accumulation. Thus, the immunohistochemical analysis of tumor tissues was employed to reveal the P-gp expression in different groups. As shown in Figure 6h, the MCP/DOC/shRNA only group (group iii) showed a lower P-gp level, compared with control group (group i) and light irradiation only group (group ii), verifying its silencing effect. When MCP/DOC/shRNA plus light irradiation (group iv, v, vi, vii), the P-gp suppression effect became more evident, implying the shRNA release could be accelerated by both 405nm and 365nm wavelength *in vivo*. Conversely, MCP/DOC/shNC had negligible effect on P-gp expression, even with any order of light irradiation. Even so, 405 nm light irradiation was more suitable for the shRNA release applications than 365 nm light irradiation, as it would guarantee the release order of gene prior to drug for optimizing and enhancing the synergistic antitumor effects through increased drug retention, based on the aforementioned *in vitro and in vivo* results.

CONCLUSIONS

In summary, we have reported a photoresponsive nanosystem of utilizing two independent light wavelength to remotely control the sequential release of shRNA and DOX for optimizing and enhancing their synergistic therapy in multidrug-resistant HepG2/ADR human liver cancer cells. We demonstrated the DOX prodrug with nitrobenzyl could be cleaved with 365 nm light rather than 405 nm, for triggering the DOX release from nanovehicles. On the other hand, we found that the shRNA packed on our nanovehicles could be rapidly released by external 405 nm light to improve P-gp suppressing effect. Taken this together, we confirmed the sequential release of shRNA and DOX regulated by an ordered exposure to light of 405 nm and 365 nm can facilitate the drug accumulation, and bring out optimized and significantly improved synergistic antitumor efficacy in HepG2/ADR cells *in*

vitro and in vivo. This work not only demonstrated the importance of the sequential release of shRNA and drug for MDR reversal, but also provided a novel strategy for precisely control the release of multiple components, such as shRNA and doxorubicin.

EXPERIMENTAL SECTION

See the Supporting Information for experimental details.

ASSOCIATED CONTENT

Supporting Information

Experimental section, FT-IR spectra, ^{1}HNMR, ^{13}CNMR, ^{13}C CP/MAS NMR, AFM images, TLC results, fluorescence intensity of DOC and DOX standard solutions, CLSM images of HepG2/ADR cells incubated with MCP/pDNA, fluorescence microscopic images of EGFP gene expression, light penetration depth results, and the photo-damage effect of light.

AUTHOR INFORMATION

Corresponding Authors:

*X. Liu. E-mail: xiaoloong.liu@gmail.com
*J. Liu. E-mail: drjingfeng@126.com

ORCID

*X. Liu: 0000-0002-3096-4981
*J. Liu: 0000-0003-3499-5678

Author Contributions:

M.W. and X.L contributed equally to this work.

Notes

The authors declare no competing financial interest.

ACKNOWLEDGEMENTS

This work is supported by the Natural Science Foundation of China (Grant No. 81671813, 81601538, U1505221, 61727823, 61575044 and 21705022); the joint research projects of

Health and Education Commission of Fujian Province (Grant No. WKJ2016-2-15); the Joint Funds for the innovation of science and Technology, Fujian province (Grant No. 2016Y9062 and 2016Y9061); the Natural Science Foundation of Fujian Province (Grant No. 2018J01144); the Scientific Foundation of the Fujian provincial Health and Family Planning Commission (Grant No. 2017-1-84 and 2017-ZQN-75); the Scientific Foundation of Fuzhou City (Grant No. 2016-S-124-3).

REFERENCES

1. Shen, J.; Wang, Q.; Hu, Q.; Li, Y.; Tang, G.; Chu, P. K. Restoration of Chemosensitivity by Multifunctional Micelles Mediated by P-gp siRNA to Reverse MDR. *Biomaterials* **2014,** *35*, 8621-8634.

2. Chen, W.; Yuan, Y.; Cheng, D.; Chen, J.; Wang, L.; Shuai, X. Co-Delivery of Doxorubicin and siRNA with Reduction and pH Dually Sensitive Nanocarrier for Synergistic Cancer Therapy. *Small* **2014,** *10*, 2678-2687.

3. Borst, P.; Evers, R.; Kool, M.; Wijnholds, J. A Family of Drug Transporters: The Multidrug Resistance-Associated Proteins. *JNCI, J. Natl. Cancer Inst.* **2000,** *92*, 1295-1302.

4. Longley, D. B.; Johnston, P. G., Molecular Mechanisms of Drug Resistance. *J. Pathol.* **2005,** *205*, 275-292.

5. Burnett, J. C.; Rossi, J. J.; Tiemann, K. Current Progress of siRNA/shRNA Therapeutics in Clinical Trials. *Biotechnol. J.* **2011,** *6*, 1130-1146.

6. Zhang, S.; Zhao, B.; Jiang, H.; Wang, B.; Ma, B., Cationic Lipids and Polymers Mediated Vectors for Delivery of siRNA. *J. Controlled Release* **2007,** *123*, 1-10.

7. Duan, X.; Xiao, J.; Yin, Q.; Zhang, Z.; Yu, H.; Mao, S.; Li, Y., Smart pH-Sensitive and Temporal-Controlled Polymeric Micelles for Effective Combination Therapy of Doxorubicin and Disulfiram. *ACS Nano* **2013,** *7*, 5858-5869.

8. Deng, Z.; Qian, Y.; Yu, Y.; Liu, G.; Hu, J.; Zhang, G.; Liu, S., Engineering Intracellular Delivery Nanocarriers and Nanoreactors from Oxidation-Responsive Polymersomes via Synchronized Bilayer Cross-Linking and Permeabilizing Inside Live Cells. *J. Am. Chem. Soc.* **2016**, *138*, 10452-10466.

9. Wang, X.; Liu, G.; Hu, J., Zhang, G.; Liu, S., Concurrent Block Copolymer Polymersome Stabilization and Bilayer Permeabilization by Stimuli-Regulated "Traceless" Crosslinking. *Angew. Chem., Int. Ed.* **2014**, *53*, 3138-3142.

10. Yao, C.; Wang, X.; Liu, G.; Hu, J.;, Zhang, G.; Liu, S., Distinct Morphological Transitions of Photoreactive and Thermoresponsive Vesicles for Controlled Release and Nanoreactors. *Macromolecules* **2016**, *49*, 8282-8295.

11. Zhu, K.; Deng, Z.; Liu, G.; Hu, J.; Liu, S., Photoregulated Cross-Linking of Superparamagnetic Iron Oxide Nanoparticle (SPION) Loaded Hybrid Nanovectors with Synergistic Drug Release and Magnetic Resonance (MR) Imaging Enhancement. *Macromolecules* **2017**, *50*, 1113-1125.

12. Xiong, X.-B.; Lavasanifar, A., Traceable Multifunctional Micellar Nanocarriers for Cancer-Targeted Co-Delivery of MDR-1 siRNA and Doxorubicin. *ACS Nano* **2011,** *5*, 5202-5213.
13. Baek, S. E.; Lee, K. H.; Park, Y. S.; Oh, D.-K.; Oh, S.; Kim, K.-S.; Kim, D.-E., RNA Aptamer-Conjugated Liposome as an Efficient Anticancer Drug Delivery Vehicle Targeting Cancer Cells In Vivo. *J. Controlled Release* **2014,** *196*, 234-242.
14. Meng, H.; Liong, M.; Xia, T.; Li, Z.; Ji, Z.; Zink, J. I.; Nel, A. E., Engineered Design of Mesoporous Silica Nanoparticles to Deliver Doxorubicin and P-gp siRNA to Overcome Drug Resistance in a Cancer Cell Line. *ACS Nano* **2010,** *4*, 4539-4550.
15. Chen, A. M.; Zhang, M.; Wei, D.; Stueber, D.; Taratula, O.; Minko, T.; He, H., Co-Delivery of Doxorubicin and Bcl-2 siRNA by Mesoporous Silica Nanoparticles Enhances the Efficacy of Chemotherapy in Multidrug-Resistant Cancer Cells. *Small* **2009,** *5*, 2673-2677.
16. Zhang, L.; Lu, Z.; Zhao, Q.; Huang, J.; Shen, H.; Zhang, Z., Enhanced Chemotherapy Efficacy by Sequential Delivery of siRNA and Anticancer Drugs Using PEI-Grafted Graphene Oxide. *Small* **2011,** *7*, 460-464.
17. Biswas, S.; Deshpande, P. P.; Navarro, G.; Dodwadkar, N. S.; Torchilin, V. P., Lipid Modified Triblock PAMAM-Based Nanocarriers for siRNA Drug Co-Delivery. *Biomaterials* **2013,** *34*, 1289-1301.
18. Agasti, S. S.; Chompoosor, A.; You, C.-C.; Ghosh, P.; Kim, C. K.; Rotello, V. M., Photoregulated Release of Caged Anticancer Drugs from Gold Nanoparticles. *J. Am. Chem. Soc.* **2009,** *131*, 5728-5729.
19. Lin, Q.; Huang, Q.; Li, C.; Bao, C.; Liu, Z.; Li, F.; Zhu, L., Anticancer Drug Release from a Mesoporous Silica Based Nanophotocage Regulated by Either a One- or Two-Photon Process. *J. Am. Chem. Soc.* **2010,** *132*, 10645-10647.
20. Beharry, A. A.; Woolley, G. A., Azobenzene Photoswitches for Biomolecules. *Chem. Soc. Rev.* **2011,** *40*, 4422-4437.
21. Jiang, J.; Tong, X.; Zhao, Y. A New Design for Light-Breakable Polymer Micelles. *J. Am. Chem. Soc.* **2005,** *127*, 8290-8291.
22. Givens, R. S.; Weber, J. F. W.; Conrad, P. G.; Orosz, G.; Donahue, S. L.; Thayer, S. A. New Phototriggers 9: p-Hydroxyphenacyl as a C-terminal Photoremovable Protecting Group for Oligopeptides. *J. Am. Chem. Soc.* **2000,** *122*, 2687-2697.
23. Canepari, M.; Nelson, L.; Papageorgiou, G.; Corrie, J. E. T.; Ogden, D. Photochemical and Pharmacological Evaluation of 7-Nitroindolinyl-and 4-Methoxy-7-Nitroindolinyl-Amino Acids as Novel, Fast Caged Neurotransmitters. *J. Neurosci. Methods* **2001,** *112*, 29-42.
24. Kantevari, S.; Passlick, S.; Kwon, H.-B.; Richers, M. T.; Sabatini, B. L.; Ellis-Davies, G. C. R. Development of Anionically Decorated Caged Neurotransmitters: In Vitro Comparison of 7-Nitroindolinyl- and 2-(p-Phenyl-o-Nitrophenyl) Propyl-Based Photochemical Probes. *ChemBioChem* **2016,** *17*, 953-961.
25. Stegmaier, P.; Alonso, J. M.; Campo, A. D. Photoresponsive Surfaces with Two Independent Wavelength-Selective Functional Levels. *Langmuir* **2008,** *24*, 11872-11879.
26. Kotzur, N.; Briand, B.; Beyermann, M.; Hagen, V. Wavelength-Selective Photoactivatable Protecting Groups for Thiols. *J. Am. Chem. Soc.* **2009,** *131*, 16927-16931.
27. San Miguel, V.; Bochet, C. G.; del Campo, A. Wavelength-Selective Caged Surfaces:

How Many Functional Levels Are Possible? *J. Am. Chem. Soc.* **2011,** *133*, 5380-5388.
28. Azagarsamy, M. A.; Anseth, K. S. Wavelength-Controlled Photocleavage for the Orthogonal and Sequential Release of Multiple Proteins. *Angew. Chem., Int. Ed.* **2013,** *52*, 13803-13807.
29. Lin, X.; Zhao, N.; Yan, P.; Hu, H.; Xu, F.-J. The Shape and Size Effects of Polycation Functionalized Silica Nanoparticles on Gene Transfection. *Acta Biomater.* **2015,** *11*, 381-392.
30. Li, X.; He, Q.; Shi, J. Global Gene Expression Analysis of Cellular Death Mechanisms Induced by Mesoporous Silica Nanoparticle-Based Drug Delivery System. *ACS Nano* **2014,** *8*, 1309-1320.
31. Oh, J.-M.; Choi, S.-J.; Lee, G.-E.; Han, S.-H.; Choy, J.-H. Inorganic Drug-Delivery Nanovehicle Conjugated with Cancer-Cell-Specific Ligand. *Adv. Funct. Mater.* **2009,** *19*, 1617-1624.
32. Karthik, S.; Puvvada, N.; Kumar, B. P.; Rajput, S.; Pathak, A.; Mandal, M.; Singh, N. P. Photoresponsive Coumarin-Tethered Multifunctional Magnetic Nanoparticles for Release of Anticancer Drug. *ACS Appl. Mater. Interfaces* **2013,** *5*, 5232-5238.
33. Hartono, S. B.; Phuoc, N. T.; Yu, M.; Jia, Z.; Monteiro, M. J.; Qiao, S.; Yu, C., Functionalized Large Pore Mesoporous Silica Nanoparticles for Gene Delivery Featuring Controlled Release and Co-Delivery. *J. Mater. Chem. B* **2014,** *2*, 718-726.
34. Żołek, T.; Paradowska, K.; Wawer, I., ^{13}C CP MAS NMR and GIAO-CHF Calculations of Coumarins. *Solid State Nucl. Magn. Reson.* **2003,** *23*, 77-87.
35. Chen, S.-C.; Kuo, S.-W.; Liao, C.-S.; Chang, F.-C., Syntheses, Specific Interactions, and pH-Sensitive Micellization Behavior of Poly[vinylphenol-b-2-(dimethylamino)ethyl methacrylate] Diblock Copolymers. *Macromolecules* **2008,** *41*, 8865-8876.
36. Zhao, N.; Lin, X.; Zhang, Q.; Ji, Z.; Xu, F. J. Redox‐Triggered Gatekeeper‐Enveloped Starlike Hollow Silica Nanoparticles for Intelligent Delivery Systems. *Small* **2015,** *11*, 6467-6479.
37. Maggini, L.; Cabrera, I.; Ruiz-Carretero, A.; Prasetyanto, E. A.; Robinet, E.; De Cola, L. Breakable Mesoporous Silica Nanoparticles for Targeted Drug Delivery. *Nanoscale* **2016,** *8*, 7240-7247.
38. Li, M.; Gao, Y.; Yuan, Y.; Wu, Y.; Song, Z.; Tang, B. Z.; Liu, B.; Zheng, Q. C. One-Step Formulation of Targeted Aggregation-Induced Emission Dots for Image-Guided Photodynamic Therapy of Cholangiocarcinoma. *ACS Nano* **2017,** *11*, 3922-3932.
39. Merdan, T.; Kopeček, J.; Kissel, T., Prospects for Cationic Polymers in Gene and OligonucleotideTherapy Against Cancer. *Adv. Drug Delivery Rev.* **2002,** *54*, 715-758.
40. Zhao, L.; Peng, J.; Huang Q.; Li, C.; Chen, M.; Sun, Y.; Lin, Q.; Zhu, L.; Li, F. Near-Infrared Photoregulated Drug Release in Living Tumor Tissue via Yolk-Shell Upconversion Nanocages. *Adv. Funct. Mater.* **2014**, 24, 363-371.
41. Babin, J.; Pelletier, M.; Lepage, M.; Allard, J.; Morris, D. A New Two-Photon-Sensitive Block Copolymer Nanocarrier. *Angew. Chem. Int. Ed.* **2009**, 48, 3329-3332.
42. Wu, M.; Wang, Q.; Liu, X.; Liu, J. Highly Efficient Loading of Doxorubicin in Prussian Blue Nanocages for Combined Photothermal/Chemotherapy Against Hepatocellular Carcinoma. *RSC Adv.* **2015,** 5, 30970-30980.
43. Zhang, D.; Zheng, A.; Li, J.; Wu, M.; Cai, Z.; Wu, L.; Wei, Z.; Yang, H.; Liu, X.; Liu, J. Tumor Microenvironment Activable Self-Assembled DNA Hybrids for pH and Redox

Dual-Responsive Chemotherapy/PDT Treatment of Hepatocellular Carcinoma. *Adv. Sci.* **2017,** *4*, 1600460.

44. Zhang, D.; Wu, M.; Cai, Z.; Liao, N.; Ke, K.; Liu, H.; Li, M.; Liu, G., Yang, H.; Liu, X.; Liu, J. Chemotherapeutic Drug Based Metal-Organic Particles for Microvesicle-Mediated Deep Penetration and Programmable pH/NIR/Hypoxia Activated Cancer Photochemotherapy. *Adv. Sci.* **2018,** *5*, 1700648.

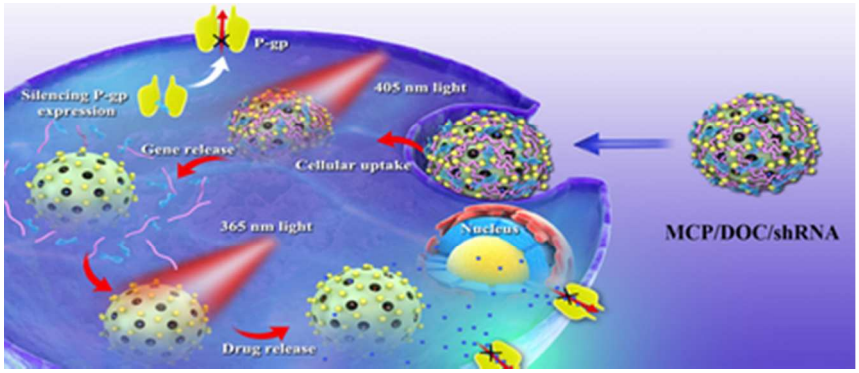

Table of Contents Graphic

35x15mm (300 x 300 DPI)